



World Conference on Transport Research - WCTR 2019 Mumbai 26-31 May 2019

Debonding detection in asphalt pavements using infrared thermography

Vidhi Vyas^a, Vedant Jagdish Patil^a, Ajit Pratap Singh^{a*}, Anshuman^a

^a Department of Civil Engineering, BITS Pilani, Pilani, 333031, India

Abstract

For sustainable growth of road networks in a country, their effective maintenance is an essential element of pavement evaluation and management strategies. Destructive testing practices are slow, labor-intensive and do not represent the entire pavement area. Advances in non-destructive testing technologies offer a convenient and reliable means of quickly scanning large areas. Infrared thermography based on capturing the thermal signature of any structure is found to be very useful for detecting pavement subsurface flaws. This study aims at exploring the potential of infrared thermography to detect subsurface interlayer debonding in asphalt pavements. An in-situ asphalt pavement test section has been constructed with different bonding conditions, and infrared thermography has been performed. A novel approach for quantitative and qualitative analyses of these thermal images has been carried out using MATLAB. Suitable time durations to perform thermographic inspections based on interchange time duration have been suggested.

© 2018 The Authors. Published by Elsevier B.V.

Peer-review under responsibility of WORLD CONFERENCE ON TRANSPORT RESEARCH SOCIETY.

Keywords: Non-destructive testing; interlayer debonding; asphalt pavements; infrared thermography; thermal images

1. Introduction

Every country requires an adequate transportation system for its economic and social development. In order to travel safely, comfortably and at design speed, it is necessary to have a proper riding surface. Thus, a properly designed and constructed pavement surface is essential for the movement of people and commodities. The primary function of pavement is to distribute the applied vehicle wheel loads to the larger area on subgrade soil. In this way, the stresses produced due to heavy wheel loads at the pavement surface are transferred at considerably lower magnitudes to the subgrade soil. An asphalt pavement transfers the vertical compressive stresses by grain-to-grain contact of the constituent aggregates, whereas a slab action, due to the high modulus of elasticity is involved in rigid pavements. The reduction in stress due to wheel loads depends on the thickness and characteristics of different pavement layers.

* Corresponding author. Tel.: +91-9664031566; fax: +91-1596-242183.

E-mail address: aps@pilani.bits-pilani.ac.in

These pavement layers must have adequate adhesion at their interfaces so that they behave as a structural monolith against traffic loading and environmental effects. Poor adhesion at these layer interfaces causes the two layers to behave as the thin individual layers and results in a phenomenon called interlayer debonding. This adversely affects the performance of pavements and gives rise to another distresses including permanent deformation, top-down cracking and eventually reduced service life.

Visual indicators of debonding in asphalt pavements include crescent-shaped slippage cracks on the surface, particularly subjected to high horizontal stresses. This problem becomes severe in the case of airfield pavements since they undergo high shear stresses by aircraft frequently during landing and turning operations. To avert any mishap, it is vital to identify the areas undergoing debonding in advance, so that suitable repair and maintenance measures could be adopted. Non-destructive testing (NDT) methods offer the best means in identification and assessment of the extent and depth of this subsurface defect, during construction, post-construction, and forensic studies.

Infrared thermography (IRT) technique has shown promising results in identifying shallow surface flaws. All bodies at a temperature over 0 K emit radiations with the wavelength proportional to their temperature and lying in the infrared portion (wavelength 0.75 μm and 1000 μm) of the electromagnetic spectrum (Solla et al., 2014). The emitted infrared radiations are detected by infrared measuring devices, and temperature of the surface is calculated based on Stefan–Boltzmann’s law, which is expressed as shown in Equation (1).

$$q/A = \varepsilon\sigma T^4 \quad (1)$$

where, q is the rate of energy emission (W), A is the area of the emitting surface (m^2), T is the absolute temperature (K), σ is the Stefan–Boltzmann’s constant ($\sigma = 5.676 \times 10^{-8} \text{ W m}^{-2} \text{ K}^{-4}$) and ε is the emissivity of the emitting surface for a fixed wavelength, and absolute temperature T . Emissivity is unity for a perfect blackbody, but it is always less than unity, for real surfaces.

Presence of subsurface anomalies, voids, cracks, and debonding in any material interrupt the heat flow through it, warm faster than surrounding areas and appear in thermal images as hot spots, during the day time. At night, they dissipate heat faster than the surrounding and appear in thermal images as cold areas (Weil, 1996). As per the ASTM specifications, ‘the minimum temperature difference of 0.5 $^{\circ}\text{C}$ between bonded and the debonded area is required to be detected by an infrared camera, with testing performed when wind speed is less than 50 kmh^{-1} ’ (ASTM D4788–03, 2013). IRT is based on two different approaches, passive and active. The passive approach makes use of thermal radiations emitted by the surface of the test body under natural conditions. Based on the anticipated depth of defect, the inspection time can vary from 5 to 9 hours, after sunrise (Washer et al., 2010). In the active approach, thermal excitation is applied by an external energy source to produce a thermal contrast between the areas of study, and the surrounding ones, either by heating or cooling the object (Milovanović and Pečur, 2016). The defect is detected due to its inconsistent heat transfer behavior. Nevertheless, various external factors such as, intensity and amount of solar radiation, maximum and minimum temperature in a day and ambient air temperature variation between day and night, affect the detection of debonding in passive approach (Malhotra and Carino, 2004).

Over the years, various researchers have successfully detected subsurface cracks, voids, and delaminations in concrete bridge components, pavements, building walls, and parking lots using IRT (Sultan and Washer, 2016; Vaghefi et al., 2011; Washer and Fuchs, 2015). IRT was reported to detect delamination up to 25.4 mm from a concrete surface (Hiasa, 2016). Verification of debonding assessment was usually done by extracting cores at the test locations (Gucunski et al., 2013). IRT has shown its potential to identify the delamination, stripping, voids and other anomalies in asphalt pavements located at shallow depths (40–70 mm) (Heitzman et al., 2013; Tsubokawa et al., 2007). However, it could not determine the depth and dimensions of the defects to the desired accuracy. Hence the use of GPR in combination with IRT was made (Moropoulou et al., 2002; Solla et al., 2014). The method is economical, repeatable, and quickly covers large areas, and thus also being widely used for airfield pavements. However, it has not been proven effective to estimate the depth and dimensions of the defect. For this purpose, it is recommended to adopt other NDT techniques for detailed investigations.

In addition to this, the availability of advanced analyses of infrared thermography images for debonding detection of pavements is still limited. Therefore, this study aims at exploring the potential of infrared thermography technique to detect debonding in asphalt pavements by carrying out quantitative and qualitative analyses of the thermal images.

2. Study objectives

The objectives of this study are to assess the potential of infrared thermography method in identifying interlayer debonding of asphalt pavements and to estimate ideal time durations for the same, based on a passive approach. Influence of different thermal conductivity material as a debonding agent on the overall thermal behavior of pavement has also been studied. In addition to this, a methodology for post-processing of thermal images to quantitatively analyze the results has been developed.

3. Experimental program

3.1. Construction of in-situ asphalt pavement test section

In order to perform controlled field non-destructive testing, an in-situ asphalt pavement test section has been constructed as an overlay on existing asphalt pavement, with 6 m × 1.8 m lateral dimensions and 150 mm thickness. Three hot-mix asphalt (HMA) lifts of 50 mm each has been laid. The test section has been divided into various blocks of 60 cm × 60 cm, as per the different bonding conditions induced in it. The different artificially constructed bonding conditions are placed at three depths of 50 mm, 100 mm and 150 mm. They include four debonding conditions using sand (no bond: 1), grease (no bond: 2), polythene (no bond: 3), and bentonite slurry (no bond: 4); one partial bonding condition using dust along the wheel paths and one full bonding condition in order to compare the results. The purpose of providing different bonding conditions is to check the influence of the bonding agent on the overall thermal behavior of the pavement. Fig. 1 depicts the plan of a part of the constructed test section (bonding conditions at 50 mm depth only) over which satisfactory testing results have been obtained. It is to be noted that bond conditions located at greater depths showed no significant thermal behavior and thus they have refrained from any further testing and analysis.

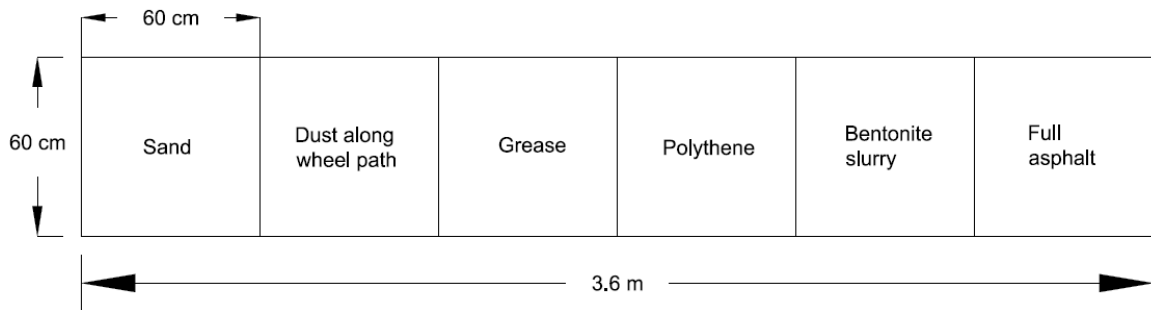


Fig. 1. Plan of constructed in-situ asphalt pavement test section showing different conditions of the interlayer bond at 50 mm depth.

3.2. Test equipment

A FLIR T250 infrared thermography camera has been utilized for taking thermal images. The camera collects and stores images of 320 × 240 pixels resolution. Table 1 summarizes some of the main technical specifications of the thermal camera (FLIR Catalog, 2009). The testing has been performed in accordance with ASTM D4788-88 standards.

Table 1. Technical specifications of FLIR T250 thermal camera.

Particulars	Specifications	Unit
Measurement object temperature range	-20 to +350	°C
Accuracy	2% of reading or ±2	°C
Thermal sensitivity at 30°C	80	mK
Field of view (FOV)	25 × 19	°
Minimum focus distance	0.4	m

Spatial resolution	2.18	mrاد
Spectral range	7.5 - 13	μm
Imaging frequency	9	Hz
IR resolution	320 × 240	pixel
Focal plane array	Uncooled microbolometer	-
Digital zoom	1–2×	-

3.3. Data collection

Data collection using infrared camera has been extensively performed over a period of one month. The images have been taken regularly block-wise, over 30 minute time intervals from 00:00 hours to 23:30 hours, with the camera aperture at the height of ~0.5 meters from the pavement surface. The images have been post-processed to interpret desired results. Due to brevity reasons, only the results of a typical sunny summer day have been presented. Table 2 presents the environmental conditions measured at the local weather station on the day of testing.

Table 2. Environmental conditions at the time of testing.

Ambient temperature range (°C)	Relative humidity range (%)	Wind speed (km/h)	Pavement temperature range (°C)
28-40	15-57	3-10	23.6-56.5

3.4. Data processing

The most common practice of thermal images analysis is by visually observing the color contrast of the images. However, this is qualitative and more of an experience-based practice. In addition to this, under natural environmental conditions of passive thermography, many times the color variation is not clearly distinguishable. This necessitates for a better and quantitative analysis approach.

In this study, data analysis has been performed in two stages. In the first step, all raw thermal images of a particular time interval have been calibrated to the same temperature scale using FLIR QuickReport software (version 1.2 SP2) (2009). Post-calibration has also been performed on the basis of the atmospheric temperature, relative humidity, acquisition height, and reflected the apparent temperature of the targets. The final output of this first phase of processing is a set of 8-bit grayscale images.

In the second stage, the analysis is performed using MATLAB. The output images of FLIR QuickReport are fed into MATLAB for further analysis. Even though the color variation between bonded and debonded images can be seen for a few time intervals in a day, for exact quantitative judgment, the temperature histogram for each debonding condition have been plotted against the temperature histogram for the full bond condition, in the same MATLAB figure. The grayscale pixel matrix has been converted to its corresponding temperature matrix by implementing Equation (2).

$$T_{ij} = T_l + P_{ij} * \frac{T_h - T_l}{256} \quad (2)$$

where T_{ij} is the temperature at the point corresponding to the pixel in the i^{th} row and j^{th} column, T_l is the calibrated minimum temperature, T_h is the calibrated maximum temperature, and P_{ij} is the grayscale intensity of the pixel in the i^{th} row and j^{th} column.

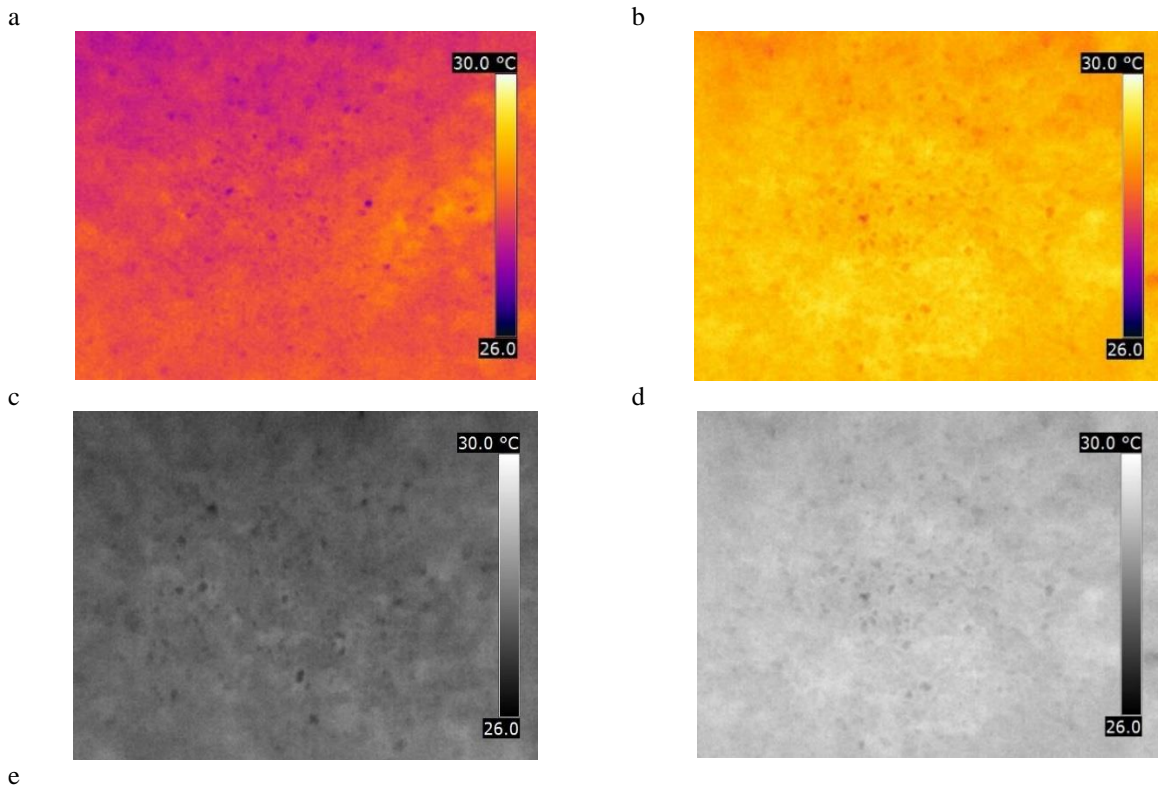
4. Results and discussion

In accordance with ASTM D4788-03 (2013), for delamination detection on concrete bridge decks, ‘the minimum temperature difference of 0.5 °C between bonded and the debonded area is required to be detected by the infrared

camera, with testing performed when wind speed is less than 50 kmh^{-1} . Even for the asphalt pavements, it has been observed to be true. Comparative histograms plotted between temperature range and pixel count of each debonded area with bonded area verify the aforementioned fact. Thermal contrast values between each debonded area with the bonded area has been calculated.

Figs. 2 to 5 present the results of thermal variation over grease debonded and bonded areas. At most of the times, the least thermal contrast has been obtained for grease debonded condition. Thus, the entire process has been comprehensively explained for grease debonded and full bonded condition.

Fig. 2 presents the images and comparative histogram for grease debonded and bonded asphalt conditions, respectively at around 02:30 hours. Fig 2a and 2b present the colored thermal images and Fig. 2c and 2d present their corresponding grayscale images. The temperature for grease debonded block lies in the range of about $27.2\text{--}28.5 \text{ }^\circ\text{C}$, and that for the bonded block is around $28.4\text{--}29.5 \text{ }^\circ\text{C}$, as seen from Fig. 2e. The thermal contrast is found to be $1.15 \text{ }^\circ\text{C}$ which is greater than $0.5 \text{ }^\circ\text{C}$, and thus makes debonded area detectable by thermal imaging camera. This trend of bonded asphalt block being relatively warmer than the grease debonded block is observed throughout the night since the debonded layer acts as an insulator and does not allow the heat flow. It causes HMA block above debonding to cool or warm faster than the fully bonded block, which undergoes slow heating and cooling.



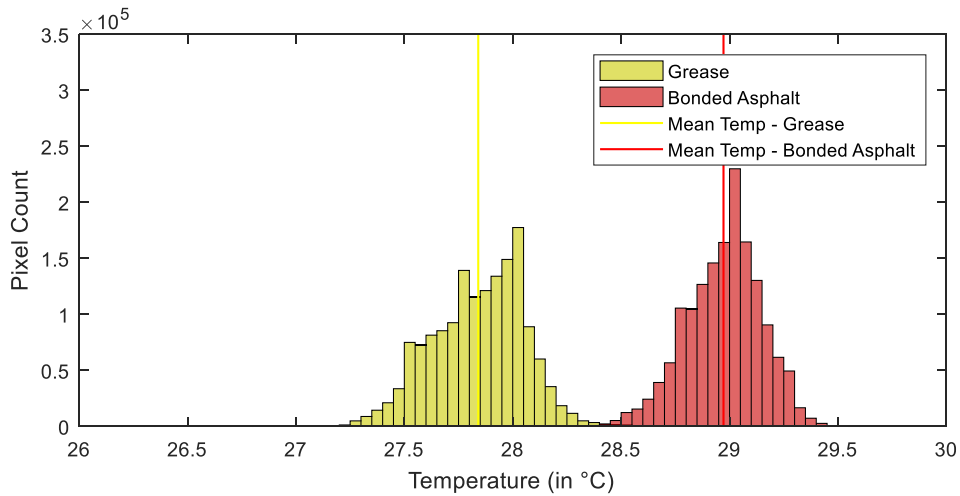
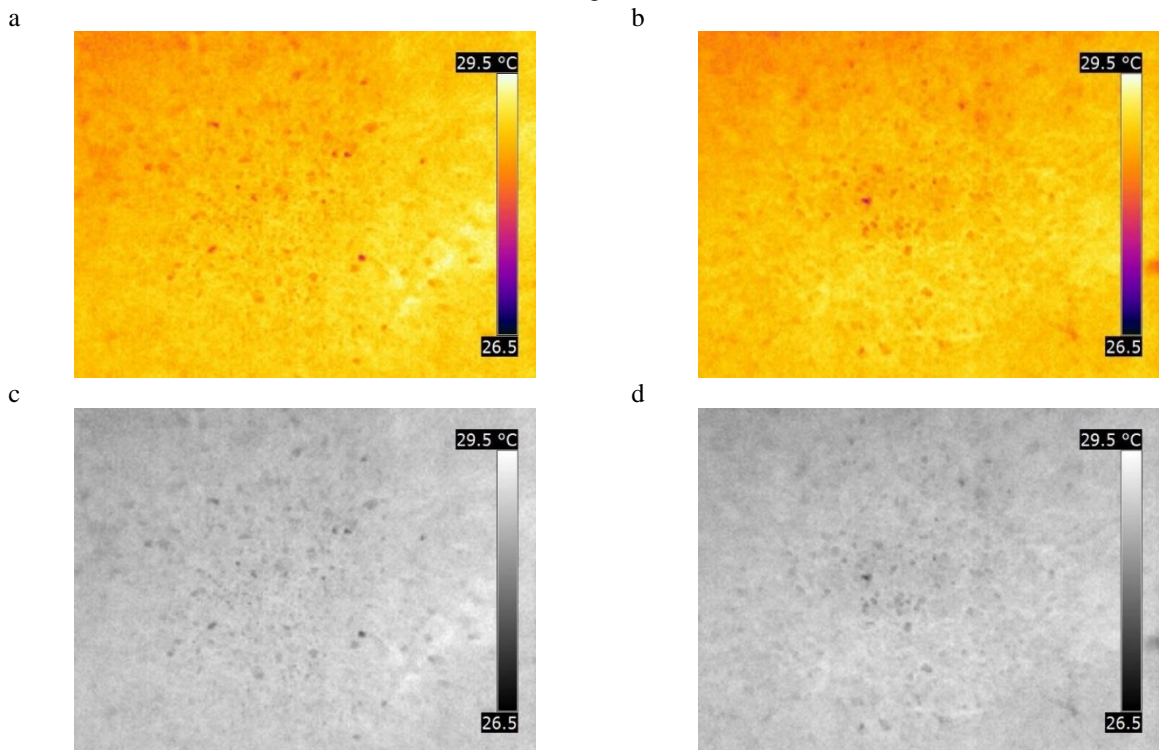


Fig. 2. (a) Raw colored thermal image of grease block; (b) Raw colored thermal image of bonded block; (c) Raw grayscale thermal image of grease block; (d) Raw grayscale thermal image of bonded block; (e) Comparative histogram of grease and bonded block at 02:30 hours.

The ambient temperature starts rising, as the sun rises. This causes heating the pavement also. Fig 3a and 3b present the colored thermal images at 07:30 hours and Fig. 3c and 3d present their corresponding grayscale images. The thermal images show almost no contrast with the pixels in both being equally bright. The temperature for both grease and asphalt blocks lie in the range of about 28.3-29.5 °C. The histograms for both as shown in Fig. 3e are observed to be merging during this time duration, and their thermal contrast is almost zero. The debonded areas go unidentified through thermal imaging camera, and infrared thermography is not found effective in detecting subsurface debonding. This trend continued for around 3.5 hours in the morning.



e

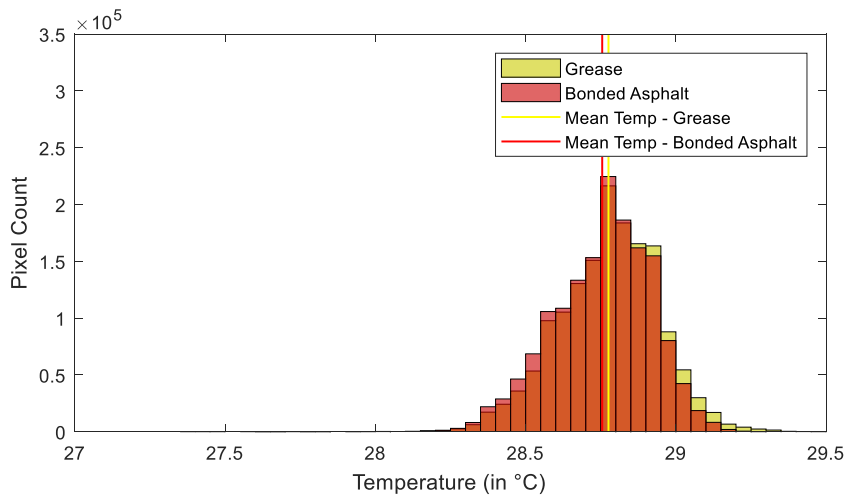
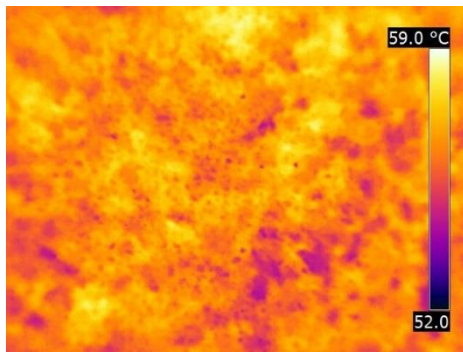


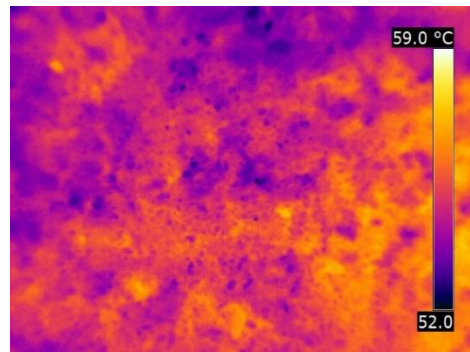
Fig. 3. (a) Raw coloured thermal image of grease block; (b) Raw coloured thermal image of bonded block; (c) Raw grayscale thermal image of grease block; (d) Raw grayscale thermal image of bonded block; (e) Comparative histogram of grease and bonded block at 07:30 hours.

As the day progresses, the increasing ambient temperature and intensity of solar radiation cause grease debonded block to heat up at a higher rate than the bonded block. At around 11:00 hours, the colored and grayscale thermal images for grease block is brighter than that for the bonded asphalt block as seen from Figs. 4a to 4d. The nature of the contrast changes and position of histograms flips on the x-axis, as shown in Fig. 4e. Grease debonded block lies in the temperature range of 54.3-58.8 °C, whereas bonded asphalt block lies in the temperature range of 53.0-57.0 °C. Thermal contrast is found to be around 1.7 °C, lying in the detectable range.

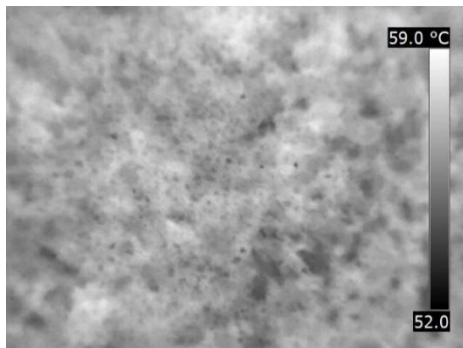
a



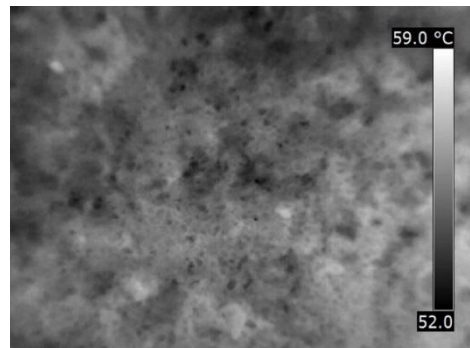
b



c



d



e

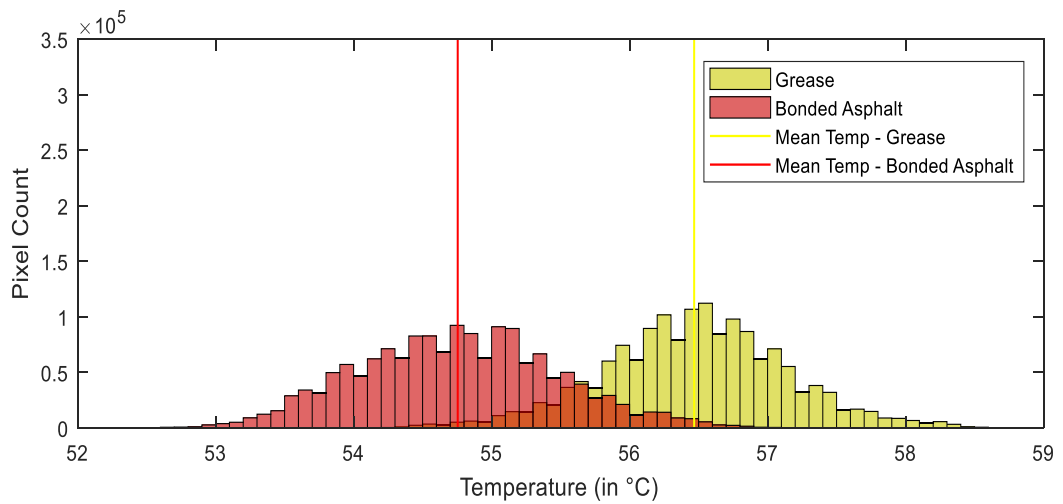
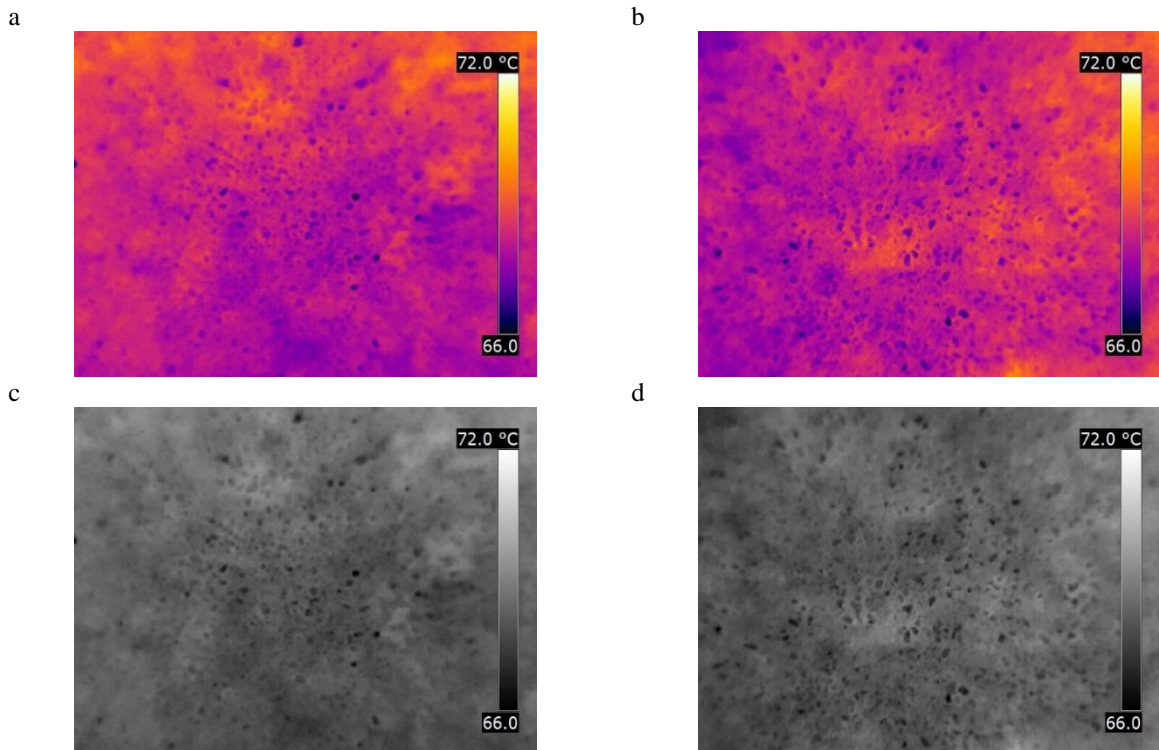


Fig. 4. (a) Raw colored thermal image of grease block; (b) Raw colored thermal image of bonded block; (c) Raw grayscale thermal image of grease block; (d) Raw grayscale thermal image of bonded block; (e) Comparative histogram of grease and bonded block at 11:00 hours.

Further, the temperature keeps rising for both the blocks. At around 15:00 hours, histograms for both of these again merge, thermal contrast becomes almost zero and the debonded areas again goes almost indistinguishable, as evident from Figs. 5a to 5e. The temperature scale of both of these lies in the range of 66.6–69.5 °C. This trend is observed to persist throughout the evening until the end of the day. Thus, its detection by the thermal camera is difficult.



e

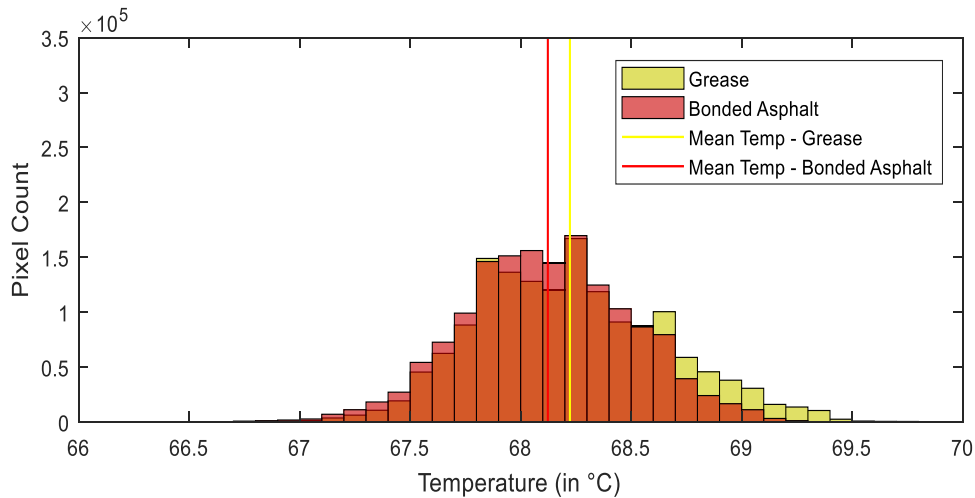


Fig. 5. (a) Raw colored thermal image of grease block; (b) Raw colored thermal image of bonded block; (c) Raw grayscale thermal image of grease block; (d) Raw grayscale thermal image of bonded block; (e) Comparative histogram of grease and bonded block at 15:00 hours.

The histograms for grease overlap with those for bonded asphalt for most of the time duration and the values of thermal contrast for grease are found to be the lowest, which makes it undetectable by a thermal camera. The interchange time zone for grease is found to be 6:30 hours to 10:00 hours in the morning and 15:00 hours to 22:00 hours in the evening. This implies that IRT will prove quite ineffective in detecting a debonding caused by grease, particularly at these durations. The values for thermal contrast are observed to be the largest for the sand debonded block, followed by dust along wheel path, polythene, bentonite, and smallest for grease debonded block. Fig. 6 shows the time durations in morning and evening when the defect goes unidentified by the thermal camera, according to the material causing debonding. It can be seen that in the entire day, the largest interchange time duration has been obtained for grease (10.5 hours), thus being most difficult to detect and least for sand (3 hours), relatively easier to detect.

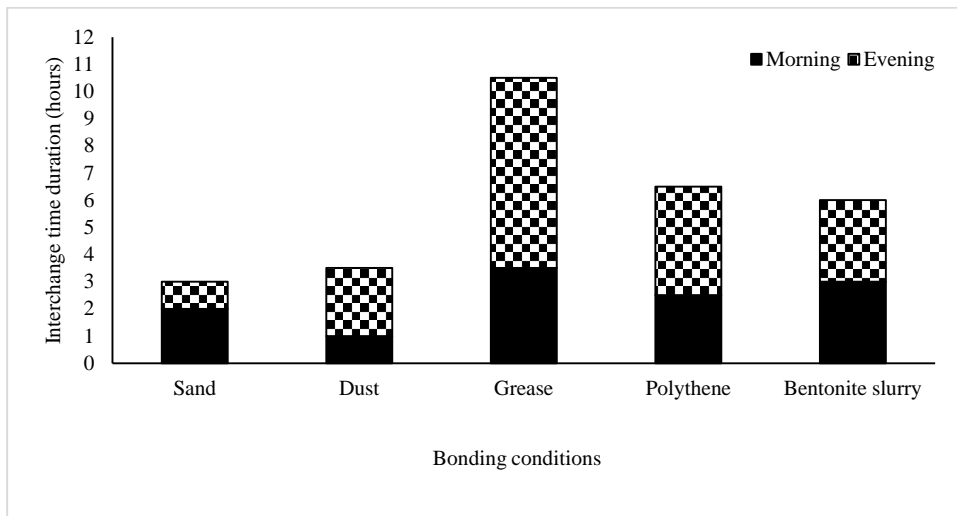


Fig. 5. Interchange time durations during morning and evening for different bonding conditions.

5. Conclusions

This study aims at assessing the potential of infrared thermography technique to detect subsurface debonding in asphalt pavement and estimating the ideal time duration for the same. For this purpose, comprehensive thermography testing has been performed over the constructed test section. The thermal images clearly show that the debonded areas are identified through the thermal imaging camera when their thermal contrast with the bonded area is greater than 0.5 °C. However, during the interchange time zone of day heating and night cooling, the debonded areas go unrecognizable through the thermal imaging camera. These interchange time zones can be seen as histograms merging with one another. It can thus be concluded that the detectability of debonding depends on the thermal conductivity of the material causing it. From the results of this experiment, for grease debonding the interchange time zones are found to be around 3.5 hours in the morning and 7 hours in the evening. Thus, the most suitable time to inspect using infrared thermography would be during night-time since debonding would be distinguishable for greater durations. The inspection can be planned accordingly.

The method suffers from inherent limitations that it could not detect the depth of flaw location and is successful only for shallow subsurface defects in asphalt pavements, up to 50 mm in this experiment, under above-mentioned conditions. Nevertheless, it is highly preferred for field inspections and data collection since it can quickly scan large areas which save labor costs and time in data collection. Also, it works only on thermal radiations, and the device itself does not emit any radiation, thus safe for the environment.

References

- ASTM D4788-03, 2013. Standard Test Method for Detecting Delaminations in Bridge Decks using Infrared Thermography, ASTM International, West Conshohocken, PA.
- FLIR T250 Catalog, 2009. Technical Data of FLIR T250 Infrared Camera. FLIR System Inc., Sweden.
- FLIR QuickReport software version 1.2 SP2, 2009. FLIR System Inc., Sweden.
- Gucunski, N., Imani, A., Romero, F., Nazarian, S., Yuan, D., Wiggemhauser, H., Shokouhi, P., Taffe, A., Kutrubes, D., 2013. Non-destructive testing to identify concrete bridge deck deterioration. Transportation Research Board, Washington DC, SHRP 2 Report S2-R06A-RR-1.
- Heitzman, M., Maser, K., Tran, N., Brown, R., Bell, H., Holland, S., Ceylan, H., Belli, K., Hiltunen, D., 2013. Non-destructive testing to identify delaminations between HMA Layers Volume 1-Summary. National Academies Press, Washington DC, SHRP 2 Report S2-R06D-RR-1.
- Hiasa, S., 2016. Investigation of infrared thermography for subsurface damage detection of concrete structures. Dissertation, University of Central Florida.
- Malhotra, V., Carino, N., 2003. Handbook on Nondestructive Testing of Concrete Second Edition. CRC press.
- Milovanović, B., Banjad Pečur, I., 2016. Review of active IR thermography for detection and characterization of defects in reinforced concrete. *Journal of Imaging* 2.2, 11.
- Moropoulou, A., Avdelidis, N., Kouli, M., Aggelopoulos, A., Karmis, P., 2002. Infrared thermography and ground penetrating radar for airport pavements assessment. *Nondestructive Testing and Evaluation* 18.1, 37-42.
- Solla, M., Lagüela, S., González-Jorge, H., Arias, P., 2014. Approach to identify cracking in asphalt pavement using GPR and infrared thermographic methods: Preliminary findings, *NDT & E International* 62, 55-65.
- Sultan, A., Washer, G., 2016. Reliability analysis of infrared thermography (IRT) for the detection of subsurface delamination, *NDE/NDT for Highways and Bridges: SMT 2016*. Portland, OR, 118-125.
- Tsubokawa, Y., Mizukami, J., Esaki, T., Hayano, K., 2007. Infrared thermographic inspection of de-bonding between layers of airport flexible pavement, 5th International Conference on Maintenance and Rehabilitation of Pavements and Technological Control. UT, 307-312.
- Vaghefi, K., Melo e Silva, H., Harris, D., Ahlborn, R., 2011. Application of thermal IR imagery for concrete bridge inspection, *PCI National Bridge Conference*. UT, 1-12.
- Washer, G., Bolleni, N., Fenwick, R., 2010. Thermographic imaging of subsurface deterioration in concrete bridges. *Transportation Research Record: Journal of the Transportation Research Board* 2201, 27-33.
- Washer, G., Fuchs, P., 2015. Developments in the use of infrared thermography for the condition assessment of concrete, *International Symposium Non-Destructive Testing in Civil Engineering (NDT-CE)*. Berlin, 281-290.
- Weil, G., 1996. Infrared thermographic techniques. *NDT & E International* 6.29, 399.